


# Competition of natural convection and thermal creep in a square enclosure

Cite as: Phys. Fluids **32**, 102001 (2020); <https://doi.org/10.1063/5.0022260>

Submitted: 20 July 2020 . Accepted: 14 September 2020 . Published Online: 01 October 2020

Jun Zhang (张俊) , Siqi Yao (姚思齐), Fei Fei (费飞), Mohammad Ghalambaz, and Dongsheng Wen (文东升)

## COLLECTIONS

Paper published as part of the special topic on [Advances in Micro/Nano Fluid Flows: In Memory of Prof. Jason Reese](#)



View Online



Export Citation



CrossMark

## ARTICLES YOU MAY BE INTERESTED IN

[Papers selected from the 8th International Symposium on Physics of Fluids, Xi'an, China, 2019](#)

Physics of Fluids **32**, 100401 (2020); <https://doi.org/10.1063/5.0027989>

[Jeffery orbits for an object with discrete rotational symmetry](#)

Physics of Fluids **32**, 081904 (2020); <https://doi.org/10.1063/5.0015056>

[Virus transmission from urinals](#)

Physics of Fluids **32**, 081703 (2020); <https://doi.org/10.1063/5.0021450>

Physics of Fluids  
Special Issue on the **Lattice Boltzmann Method**

SUBMIT TODAY!




# Competition of natural convection and thermal creep in a square enclosure

Cite as: Phys. Fluids 32, 102001 (2020); doi: 10.1063/5.0022260

Submitted: 20 July 2020 • Accepted: 14 September 2020 •

Published Online: 1 October 2020



Jun Zhang (张俊),<sup>1,a)</sup>  Siqi Yao (姚思齐),<sup>1</sup> Fei Fei (费飞),<sup>2,a)</sup> Mohammad Ghalambaz,<sup>1</sup> and Dongsheng Wen (文东升)<sup>1,3</sup>

## AFFILIATIONS

<sup>1</sup>School of Aeronautic Science and Engineering, Beihang University, Beijing 100191, People's Republic of China

<sup>2</sup>School of Aerospace Engineering, Huazhong University of Science and Technology, 430074 Wuhan, China

<sup>3</sup>School of Chemical and Process Engineering, University of Leeds, Leeds LS2 9JT, United Kingdom

**Note:** This paper is part of the Special Topic on Advances in Micro/Nano Fluid Flows: In Memory of Prof. Jason Reese.

**a) Authors to whom correspondence should be addressed:** [jun.zhang@buaa.edu.cn](mailto:jun.zhang@buaa.edu.cn) and [ffeif@hust.edu.cn](mailto:ffeif@hust.edu.cn)

## ABSTRACT

Although natural convection and thermal creep have been well recognized in the continuum and rarefied regimes, respectively, the study of the competition of them in a wide flow regime is very scarce. From a theoretical point of view, natural convection can be described by Navier–Stokes–Fourier (NSF) equations at the macroscopic level, while thermal creep needs descriptions at the molecular level. Therefore, it is quite challenging to capture these two effects simultaneously. In this work, we employ the unified stochastic particle Bhatnagar–Gross–Krook (USP-BGK) method to investigate thermally driven gas flow in a square enclosure. The simulation results obtained by the USP-BGK method are validated by comparing to those from NSF solutions and direct simulation Monte Carlo method for the continuum and transitional regimes, respectively. We find that the flow patterns in the whole flow regime cannot be determined by just one nondimensional parameter, i.e., the Rayleigh number ( $Ra$ ), but needs two nondimensional parameters, i.e., the Knudsen number ( $Kn$ ) and the Froude number ( $Fr$ ), or  $Kn$  and  $Ra$ . Specifically, small Knudsen and Froude numbers tend to generate natural convection, while large Knudsen and Froude numbers tend to cause thermal creep. Moreover, our simulation results and analyses demonstrate that when  $Kn < 0.12$ , thermal creep is dominant if  $Ra < 1.0$ , while natural convection is dominant if  $Ra/Fr > 0.28$ , or equivalently,  $L/L^* > 1.0$ , where  $L$  is the characteristic length of the system and  $L^*$  is the equivalent characteristic length of molecules. These findings provide useful guidance for better understanding of the complex gas flows resulting from the competition of natural convection and thermal creep under microscale or low-density conditions such as on Mars.

Published under license by AIP Publishing. <https://doi.org/10.1063/5.0022260>

## I. INTRODUCTION

Natural convection is a type of heat and mass transport phenomenon in which the fluid motions are generated by density differences in the fluid occurring due to temperature non-uniformity. It has received sustained interest due to its ubiquitous existence in nature and a wide variety of engineering applications, such as electronic device cooling, solar thermal engineering, material processing, and nuclear engineering.<sup>1</sup> The simplest model of natural convection is a fluid layer confined between two parallel walls maintained at different temperatures. Generally, it can be classified into vertical convection and horizontal convection, depending on the relative direction of the gravity and temperature gradient. A vast

amount of research has been devoted to predicting the characteristics of fluid flow and heat transfer in these two types of natural convection.<sup>2</sup>

It is well known that in the case of vertical convection, also referred to as Rayleigh–Bénard convection, macroscopic fluid motions and convective heat transfer only occur when the imposed temperature gradient exceeds a certain value. The Rayleigh number ( $Ra$ ) at this condition is commonly called critical  $Ra$ . For the case of fluids confined between two horizontal parallel walls that are heated from below, the linear stability analysis based on Navier–Stokes–Fourier (NSF) equations predicts a critical  $Ra$  of 1708, above which pairs of counter-rotating vortices are formed.<sup>3</sup> On the contrary, there is no critical  $Ra$  for the horizontal convection.

Specifically, a circulation consisting of rising fluids along the heated wall and descending fluids along the cold wall is always formed, as long as there is a temperature gradient in a direction perpendicular to gravity.

It should be noted that the aforementioned conclusions are accurate for the continuum regime, while they may become problematic for the rarefied regime, where the nonequilibrium gas effect plays an important role. The extent of nonequilibrium can be defined by a non-dimensional parameter, namely, the Knudsen number ( $Kn$ ), which is the ratio of the molecular mean free path to the characteristic length of the system. Generally, the flow regimes can be classified as the continuum regime ( $Kn < 0.001$ ), slip regime ( $0.001 < Kn < 0.1$ ), transition regime ( $0.1 < Kn < 10$ ), and free molecular regime ( $Kn > 10$ ). Note that the demarcation between two neighboring regimes is not very strict. For example, a few studies demonstrated that the flow could be considered in the continuum regime if  $Kn < 0.01$ . Stefanov *et al.*,<sup>4,5</sup> Manela and Frankel,<sup>6,7</sup> and Zhang *et al.*<sup>8–10</sup> have reported that the Knudsen number, namely, the effect of rarefaction, also plays an important role in determining the instability of Rayleigh–Bénard convection.

In the slip and transition regime, there is a unique phenomenon called thermal creep, which results from the presence of temperature gradients along the walls rather than normal to the walls. The creep mechanism cannot be described by continuum theories but requires the viewpoint from the kinetic theory.<sup>11</sup> Considering a wall with a temperature gradient parallel to the surface, the total tangential momentum of the molecules reflected from a given point at the surface is statistically equal to zero, while the incident molecules coming from a hot region impart larger tangential momentums to the surface than those coming from a cold region. Consequently, a shear stress is exerted on the wall, with the gas flowing from the cold to the hot region as a reaction force.<sup>12</sup> Papadopoulos and Rosner<sup>13</sup> first studied gas flows generated by thermal creep in a rectangular enclosure, where the top and bottom walls were kept at different temperatures, and a linear temperature profile was assumed along the two side walls. They observed two main counter-rotating vortices with a mass flow from the cold region to the hot one in the vicinity of the side walls. Afterward, many studies have been conducted on the gas flows in cavities and channels with different geometrical configurations and different temperature distributions along the walls.<sup>10,14–18</sup>

During the past two decades, there has been ever-increasing research interest in thermal creep with the advent of micro-electro-mechanical systems (MEMS). A variety of Knudsen pumps, sensors, and actuators have been developed utilizing the effect of thermal creep.<sup>19–26</sup> Recently, de Beule *et al.*<sup>27</sup> predicted that it is possible to generate thermal creep gas flows through the porous soil in Mars due to the temperature gradients provided by local and temporal variations in solar insolation and low gas pressure. In this case, the martian soil virtually acts as a Knudsen pump, and this may be the reason for the frequent dust storms on Mars.<sup>28</sup> On the other hand, natural convection is also ubiquitous on Mars and even more intense than that on the Earth, as reported in the literature.<sup>29,30</sup> Therefore, it is interesting to study the competition of natural convection and thermal creep under some specific conditions such as microscale or low-density flows, where these two effects may play important roles simultaneously.

In the present paper, we numerically study the gas flow and heat transfer in a square enclosure, where the left and right walls are kept at different temperatures, and linear temperature distributions are assumed along both the top and bottom walls. In this model, thermal creep is caused by the temperature gradient along the top and bottom walls, and the magnitude of creep velocities is dependent on the Knudsen number. Note that gravity is also included, so natural convection (horizontal convection) is spontaneously triggered due to the temperature gradient between the left and right walls, and the magnitude of convective velocities is proportional to the Rayleigh number. Our aim is to obtain a thorough understanding of the characteristics of flow and heat transfer in enclosures for a wide range of Knudsen and Rayleigh numbers. To the best of our knowledge, there has been almost no research devoted to the combined effects of natural convection and thermal creep, except that Weng and Chen<sup>31</sup> studied the effect of thermal creep on the natural convective gas flow in a vertical open-ended parallel-plate microchannel. They found that thermal creep enhanced the flow rate and heat transfer rate, but the flow patterns did not change much as the microchannel is open-ended in their model. On the contrary, the present results demonstrate that the competition between natural convection and thermal creep makes the flow in an enclosure much more complicated, and the flow patterns are dependent on both Knudsen and Rayleigh numbers.

Simulating gas flows in enclosures covering a wide flow regime is quite challenging. It is commonly accepted that the NSF equations with no-slip or slip boundary conditions are trustable to describe gas behaviors for the continuum regime and slip regime, respectively. Correspondingly, the conventional computational fluid dynamics (CFD) methods are applicable in these flow regimes. However, when the gas flow goes to the transition and free molecular regimes, the NSF equations with linear constitutive models break down, and thus, conventional CFD calculations are no longer valid. Instead, the direct simulation Monte Carlo (DSMC) method<sup>11</sup> at the molecular level has been proved to be an efficient and accurate method under this condition. Theoretically, DSMC is valid for the whole flow regimes, as it can be regarded as a particle simulation method of solving the Boltzmann equation based on the kinetic theory. However, it is required that the cell sizes and time steps in DSMC need to be smaller than the mean free path and mean collision time, respectively.<sup>32</sup> Therefore, the application of DSMC to the continuum regime is computationally too expensive and sometimes inaccessible.

In this work, a new multiscale method called unified stochastic particle Bhatnagar–Gross–Krook (USP-BGK),<sup>33</sup> which was developed by the authors lately, is employed to simulate thermal-driven gas flows in enclosures in a wide range of Knudsen and Rayleigh numbers. Compared with DSMC, the USP-BGK method can be implemented using much larger time steps and cell sizes by coupling the effects of molecular movements and collisions. We have successfully applied it to a variety of multiscale gas flows,<sup>33</sup> and here, it is extended to simulate thermal-driven flows.

## II. SIMULATION MODEL AND NUMERICAL METHOD

Figure 1 shows a schematic diagram of our simulation model. The argon gas is confined in a square enclosure with a side length of 100 m. The left and right walls are kept at different constant

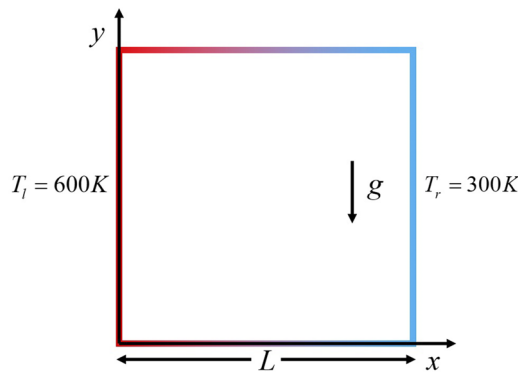


**FIG. 1.** Schematic diagram of argon gas confined in a square enclosure with temperature gradients along the horizontal direction.

temperatures, i.e.,  $T_l = 600$  K and  $T_r = 300$  K, and linear temperature distributions are assumed along both the top and bottom walls. All the walls are assumed to be of fully diffuse reflection,<sup>11</sup> which means that molecules colliding with a wall are reflected with velocities sampled randomly from a half-range Maxwellian distribution at the temperature of the specific colliding position. The gravity acceleration is downward in the vertical direction.

Note that in the continuum regime, natural convection spontaneously sets in as long as there is a temperature gradient in the direction perpendicular to gravity. For the simulation model considered in Fig. 1, a clockwise vortex is formed with the gas ascending along the left wall and descending along the right wall. The magnitude of natural convection in the continuum regime can be quantified using the Rayleigh number

$$Ra = \frac{\alpha g \Delta T L^3}{\nu \kappa}, \quad (1)$$

where  $\alpha$ ,  $\nu$ , and  $\kappa$  are the isobaric thermal expansion, kinematic viscosity, and thermal diffusivity coefficients, respectively,  $g$  is the acceleration of gravity,  $L$  is the height of the fluid layer, and  $\Delta T$  is the temperature difference between the left and right walls.

On the other side, in the slip and transition regimes, the thermal creep mechanism caused by the temperature gradient along the walls also plays an important role. In this case, gas flow from the cold region (left) to the hot region (right) is formed in the vicinity of the bottom and top walls. The magnitude of thermal creep is dependent on the Knudsen number. The competition between natural convection and thermal creep makes the flow patterns in the square enclosure complicated. To determine the specific flow state, it is required to use two nondimensional parameters in the whole flow regime rather than one counterpart in the continuum regime.

Following the previous studies for the Rayleigh–Bénard flow,<sup>4,34</sup> we expressed the Rayleigh number in terms of the Knudsen number and Froude number. Specifically, based on the state equation of a perfect gas, the isobaric thermal expansion coefficient is dependent on temperature as

$$\alpha = \frac{1}{V} \left( \frac{\partial V}{\partial T} \right)_p = \frac{1}{T}, \quad (2)$$

where  $V$  denotes the volume of gas and  $p$  is the pressure.

According to the kinetic theory, for a variable hard-sphere (VHS) gas model employed in this work, the viscosity and thermal diffusivity coefficients can be expanded as<sup>11</sup>

$$\nu = \frac{15\sqrt{\pi}}{2(7-2\omega)(5-2\omega)} \lambda c_m, \quad (3)$$

$$\kappa = \frac{45\sqrt{\pi}}{4(7-2\omega)(5-2\omega)} \lambda c_m, \quad (4)$$

where  $\lambda$  is the molecular mean free path,  $c_m$  is the most probable molecular thermal speed at the temperature  $T$ , i.e.,  $c_m = \sqrt{2RT}$ ,  $R$  is the specific gas constant, and  $\omega$  is the index of viscosity for the VHS model. In this work,  $\omega$  is set to 0.81 for argon gas.<sup>11</sup> Consider that density and temperature fields are not uniform in the enclosure. We use the average temperature and mean free path in the flow field to estimate the average thermal expansion, viscosity, and thermal diffusivity coefficients, which are defined in Eqs. (2)–(4). Substituting Eqs. (2)–(4) into Eq. (1) yields

$$Ra = \frac{32(7-2\omega)^2(5-2\omega)^2}{675\pi} \frac{1-r}{(1+r)^2 Kn^2 Fr}, \quad (5)$$

where the temperature ratio is  $r = T_r/T_l$ , the Knudsen number is  $Kn = \lambda/L$ , the Froude number is  $Fr = C_l^2/gL$ , and  $C_l$  is the most probable molecular thermal speed at the temperature  $T_l$ . Note that  $C_l$  is used in the definition of the Froude number in order to make the form of Eq. (5) consistent with the previous definition for the Rayleigh number.<sup>4</sup> Specifically, Eq. (5) automatically degrades to that defined for hard sphere (HS) gas<sup>4</sup> if the viscosity index is set to 0.5.

One successful simulation tool for capturing the thermal creep mechanism is the DSMC method proposed by Bird.<sup>11</sup> In the DSMC method, the molecular motions and inter-molecular collisions are assumed to be uncoupled in a small time step and are simulated sequentially. Macroscopic gas properties, such as density, velocity, and temperature, are obtained by sampling corresponding molecular information and making an average at the computational cells.<sup>35,36</sup> Although the DSMC method can be applied to the simulation of gas flows in the whole flow regimes, its usage is limited by cell sizes and time steps, which should be smaller than the molecular mean free path and mean collision time, respectively, to ensure its accuracy. Therefore, DSMC is computationally inefficient in the continuum regime. Since we investigate thermally induced gas flows in a wide range of Knudsen numbers in this work, a simulation method that is accurate and efficient for the whole flow regimes is required.

The unified stochastic particle method based on the Bhatnagar–Gross–Krook model (USP-BGK) is employed in the present work. The USP-BGK method was proposed by the authors recently and has been successfully applied to the whole flow regimes with the same accuracy but higher efficiency in the continuum and slip regimes compared to the DSMC method.<sup>33</sup> Here, we just provide a brief description of the basic algorithm of the USP-BGK method, and refer the reader to the original paper<sup>33</sup> for details.

Analogous to the conventional stochastic particle BGK (SP-BGK) method, the USP-BGK method employs the splitting scheme



TABLE I. Outline of the implementation of the USP-BGK method.

1. Initialization	Assign initial simulation particles in the computational domain (similar to DSMC).
2. Transport	Introduce auxiliary PDFs and move simulation particles with their velocities and apply boundary conditions to obtain $\tilde{f}^*(\mathbf{c}; \mathbf{x}, \Delta t)$ [Eqs. (10)–(12)]. Due to the gravity $g$ , the velocity of each particle has an increment of $g\Delta t$ in each time step.
3. Collision	$N_c(1 - e^{-Pr\Delta t/\tau})$ simulation particles are randomly selected to assign new velocities; the velocities of the remaining particles are unchanged [Eq. (13)].
4. Sampling	Sample the macroscopic quantities (similar to DSMC).

to solve the BGK equation in a time step by two sequential steps, i.e., the transport step and collision step, as follows:

$$\frac{\partial f^*}{\partial t} + c_i \frac{\partial f^*}{\partial x_i} = J_{(USP-BGK)}^*, \quad (6)$$

$$\frac{\partial f}{\partial t} = \frac{Pr}{\tau} (f_G - f) - J_{(USP-BGK)}^*, \quad (7)$$

where  $f^*(\mathbf{c}; \mathbf{x}, \Delta t)$  and  $f(\mathbf{c}; \mathbf{x}, \Delta t)$  are the distribution functions in the transport and collision steps, respectively.  $f_G$  is the Gaussian distribution function at equilibrium,  $Pr$  is the Prandtl number, and  $\tau = \mu/p$  is the relaxation time of the BGK model. Compared to the SP-BGK method, a modified BGK collision term  $J_{(USP-BGK)}^*$  is supplemented in Eqs. (6) and (7) to couple the molecular motion and collision effects, and it has the form

$$J_{(USP-BGK)}^* = \frac{P_c}{\tau} (f_e - f_{Grad}), \quad (8)$$

where  $f_{Grad}$  is the 13 moments Grad's distribution function,

$$f_{Grad} = f_{13} = f_e \left[ 1 + \frac{\sigma_{ik} m C_{<i} C_{k>}}{2p k_B T} + \frac{2}{5} \frac{m q_k}{p k_B T} Pr C_k \left( \frac{m C^2}{2k_B T} - \frac{5}{2} \right) \right], \quad (9)$$

where  $p$ ,  $\sigma_{ij}$ , and  $q_i$  are pressure, shear stress, and heat flux, respectively,  $f_e$  is the Maxwellian distribution at equilibrium,  $m$  is the molecule mass, and  $k_B$  is the Boltzmann constant.  $\mathbf{C} = \mathbf{c} - \mathbf{u}$  is the peculiar molecular velocity, where  $\mathbf{c}$  is the molecule velocity and  $\mathbf{u}$  is the mean velocity.  $C_{<i} C_{k>}$  denotes the symmetric and trace-free part of the tensor  $C_i C_j$ . Note that in Eq. (8),  $P_c$  is a parameter representing the degree of continuum, i.e.,  $P_c = e^{-Kn_{GLL,MAX}/Kn_c}$ , where  $Kn_c$  is a reference Knudsen number (set as 0.1 in the present work) and  $Kn_{GLL,MAX}$  is the maximum value of the gradient-length local (GLL) Knudsen number suggested by Wang and Boyd.<sup>37</sup> It indicates that  $P_c \rightarrow 1$  corresponds to the continuum limit and  $P_c \rightarrow 0$  corresponds to the free molecular limit. With this formulation, the term on the right-hand side of Eq. (6), i.e.,  $J_{(USP-BGK)}^*$ , virtually considers the collision effect in the continuum regime, while the combined effect of those two terms on the right-hand side of Eq. (7) considers the collision effect far from equilibrium.

Similar to the DSMC method, each simulation particle in the USP-BGK method is initially assigned position and velocity according to the initial conditions of the flow field. The key point of the USP-BGK method is how to implement particle transport and collision steps following the governing equations provided in Eqs. (6) and (7). Specifically, with the initial distribution function  $f(\mathbf{c}; \mathbf{x}, 0)$ ,

the transport step is numerically calculated using the solution along the characteristic line as

$$f^*(\mathbf{c}; \mathbf{x}, \Delta t) = f(\mathbf{c}; \mathbf{x} - \mathbf{c}\Delta t, 0) + \frac{\Delta t}{2} [J_{(USP-BGK)}^*(\mathbf{c}; \mathbf{x}, \Delta t) + J_{(USP-BGK)}^*(\mathbf{c}; \mathbf{x} - \mathbf{c}\Delta t, 0)]. \quad (10)$$

Note that the trapezoidal rule is used for the collision term. By introducing two auxiliary PDFs

$$\tilde{f}^* = f^* - \frac{\Delta t}{2} J_{(USP-BGK)}^*, \quad (11a)$$

$$\hat{f} = f + \frac{\Delta t}{2} J_{(USP-BGK)}^*, \quad (11b)$$

then, Eq. (10) can be rewritten as

$$\tilde{f}^*(\mathbf{c}; \mathbf{x}, \Delta t) = \hat{f}(\mathbf{c}; \mathbf{x} - \mathbf{c}\Delta t, 0). \quad (12)$$

Accordingly, the transport step can be implemented easily by just tracking simulation particles with an initial distribution function  $\hat{f}(\mathbf{c}; \mathbf{x}, 0)$ .

The obtained distribution function  $f^*(\mathbf{c}; \mathbf{x}, \Delta t)$  in the transport step is then taken as the initial condition for the collision step, and the integral solution of Eq. (7) during a time interval  $[0, \Delta t]$  gives

$$f(\mathbf{c}; \mathbf{x}, \Delta t) = f^*(\mathbf{c}; \mathbf{x}, \Delta t) e^{-Pr\Delta t/\tau} + \left( 1 - e^{-Pr\Delta t/\tau} \right) \times [f_G^*(\mathbf{c}; \mathbf{x}, \Delta t) - \tau J_{(USP-BGK)}^*(\mathbf{c}; \mathbf{x}, \Delta t)/Pr]. \quad (13)$$

It means that, in a computational cell with  $N_c$  particles, the velocities of  $N_c(1 - e^{-Pr\Delta t/\tau})$  particles need to be resampled from the distribution  $f_G^*(\mathbf{c}; \mathbf{x}, \Delta t) - \tau J_{(USP-BGK)}^*(\mathbf{c}; \mathbf{x}, \Delta t)/Pr$ , while the velocities of the remaining particles remain constant.

In summary, the USP-BGK method can be implemented in a way similar to DSMC, as shown in Table I.

### III. RESULTS AND DISCUSSIONS

In this section, gas flows in a square enclosure with a thermal gradient and gravity effect are simulated using the USP-BGK method. The obtained results are compared to the Navier–Stokes–Fourier (NSF) solutions and DSMC results for the continuum regime and rarefied regime, respectively, to validate the applicability of the USP-BGK method. Then, we employ it to study the competition of natural convection and thermal creep for a wide range of  $Kn$  and  $Fr$ . Based on simulation results, the  $(Kn, Fr)$  plane is

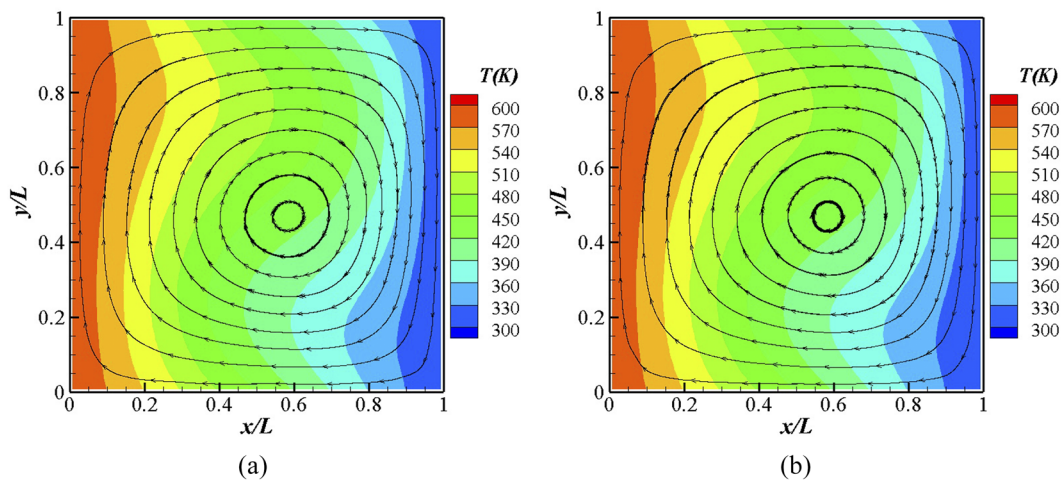


FIG. 2. Temperature contours and streamlines for  $Kn = 0.0012$  and  $Fr = 250.0$  obtained by the USP-BGK method (a) and CFD method (b).

classified into typical domains of different flow patterns, and the corresponding theoretical criteria are provided.

### A. Validation

We first validate the applicability of the USP-BGK method to the gas flows in the continuum regime by comparing its results with those obtained by the CFD method based on the NSF equations. The geometry and the wall temperature distributions are the same as described in Sec. II, and the gravity acceleration is  $10 \text{ m/s}^2$ . Consequently, the Froude number is 250.0. The gas density at the initial time instant of the simulation is  $7.16 \times 10^{-7} \text{ kg/m}^3$ , and hence, the global Knudsen number is 0.0012, which can be roughly regarded as in the continuum regime. In the NSF equations, the viscosity and thermal conductivity coefficients are assumed to be  $\mu_{ref}(T/T_{ref})^\omega$  and  $k_{ref}(T/T_{ref})^\omega$ , respectively, where  $\mu_{ref} = 2.117$

$\times 10^{-5} \text{ Pa s}$  and  $k_{ref} = 0.0165 \text{ W/(m K)}$  are the corresponding values of transport properties for argon gas at the reference temperature  $T_{ref} = 273 \text{ K}$ . This implementation ensures consistency with the USP-BGK method based on the kinetic theory. The CFD solutions are obtained using Fluent 19.2 with the velocity-pressure coupling method and laminar compressible model. Both momentum and energy equations are solved using the first-order upwind scheme. For the sake of comparison, the computational grids for both methods are set to  $72 \times 72$ , and the time step is set to  $10^{-4} \text{ s}$ . Note that the cell size is about 11.6 times of the molecular free path, and the time step is about 3.5 times of the molecular mean collision time. This is the key advantage of the USP-BGK method compared to DSMC method in which the cell size and time step should be less than the molecular mean free path and mean collision time, respectively.

Figure 2 shows the temperature contours and the streamlines obtained by the USP-BGK method and CFD method. Note that the

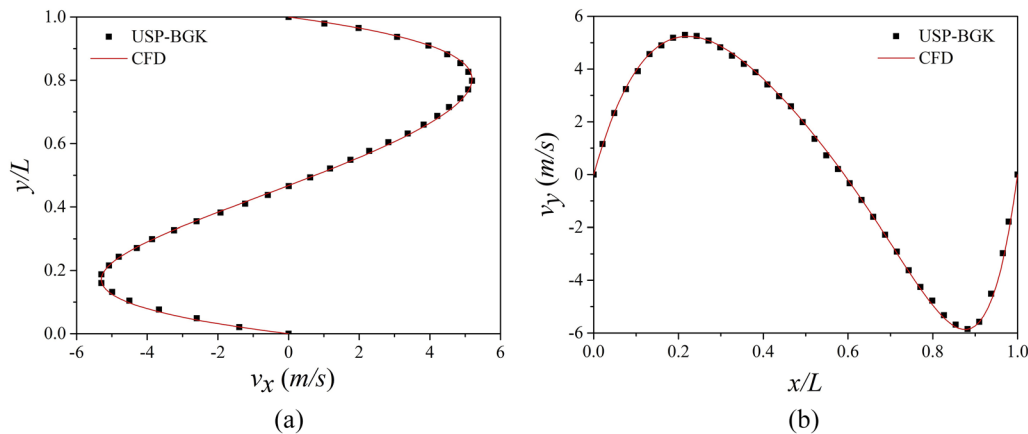


FIG. 3. Horizontal velocity along with the vertical centerline (a) and vertical velocity along the horizontal centerline (b) for  $Kn = 0.0012$  and  $Fr = 250.0$  obtained by the USP-BGK method and CFD method.

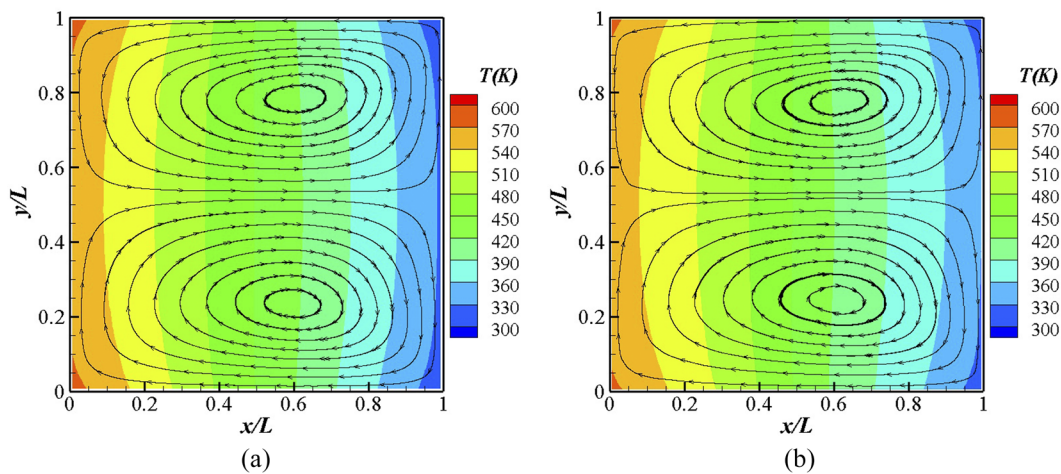


FIG. 4. Temperature contours and streamlines for  $Kn = 0.12$  and  $Fr = 250.0$  obtained by the USP-BGK method (a) and DSMC method (b).

coordinates ( $x$  and  $y$ ) of the figures in the present work are normalized by the characteristic length ( $L$ ). It can be seen that both methods predict a clockwise vortex in the field, and this is the typical phenomenon of natural convection in the continuum regime. Due to the existence of convection, the temperature distributions along the vertical direction in the field are no longer uniform, and the results predicted by these two methods agree well with each other. Figure 3 shows the comparisons of horizontal velocity along the vertical centerline and vertical velocity along the horizontal centerline. It can be concluded that the results obtained by the USP-BGK method are consistent with the solutions of NSF equations.

We then validate the applicability of the USP-BGK method to the gas flows in the transitional regime by comparing its results with those obtained by the DSMC method. The Froude number is also 250.0 as that for the continuum regime, and the gas density at the initial time instant of the simulation is changed to  $7.16 \times 10^{-9} \text{ kg/m}^3$ ,

and hence, the Knudsen number is 0.12. The computational cells for both methods are also  $72 \times 72$ , and the time step is set to  $10^{-3} \text{ s}$ . In this case, the computational cells are 0.12 times the molecular mean free path, and the time step is 0.035 times the molecular mean collision time.

Figure 4 shows the temperature contours and the streamlines obtained by the USP-BGK method and DSMC method. It can be seen that both methods predict a pair of vortices, with a flow from the cold side to the hot side in the vicinity of the top and bottom walls. This kind of flow is caused by thermal creep, which is a typical phenomenon in the rarefied regime. Figure 5 shows the horizontal velocity along the vertical centerline and vertical velocity along the horizontal centerline obtained by the USP-BGK method and DSMC method, and they agree well with each other. It can be concluded that the USP-BGK method is also capable of simulating thermal-driven gas flows in the rarefied regime.

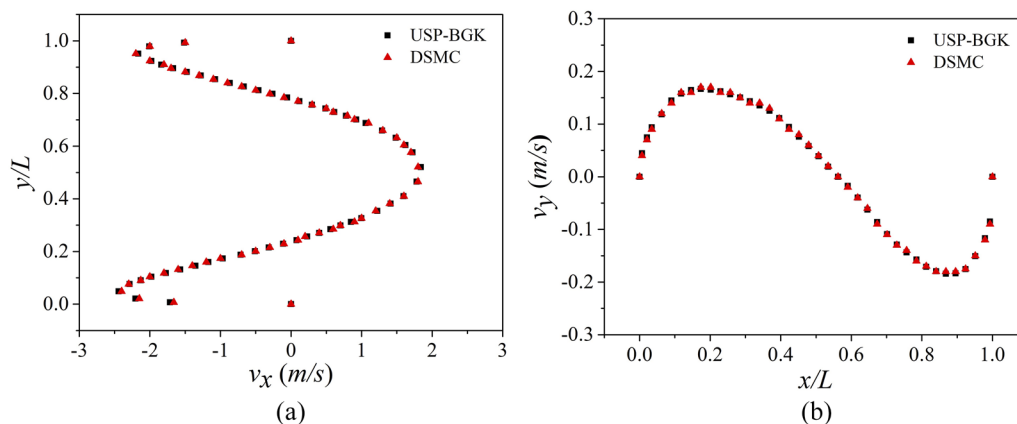
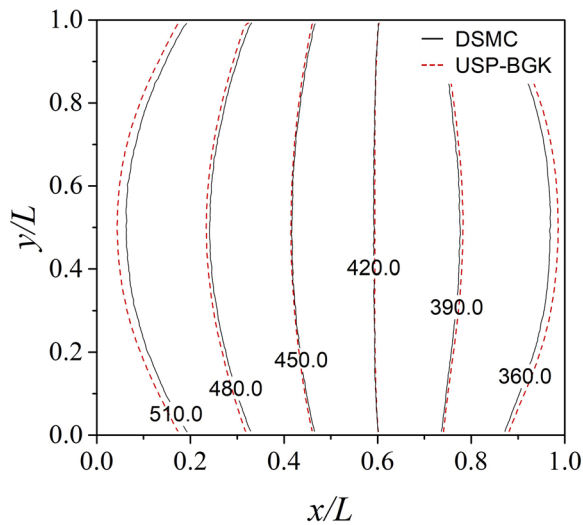


FIG. 5. Horizontal velocity along the vertical centerline (a) and vertical velocity along the horizontal centerline (b) for  $Kn = 0.12$  and  $Fr = 250.0$  obtained by the USP-BGK method and DSMC method.



**FIG. 6.** Isotherms for  $Kn = 1.2$  and  $Fr = 250.0$  obtained by the USP-BGK and DSMC methods.

We further extend our simulations to larger Knudsen numbers. Figure 6 shows the isotherms for  $Kn = 1.2$  obtained by the USP-BGK and DSMC methods. It can be seen that the deviation between these two results is larger than that for  $Kn = 0.12$ . By far, the applicability of the ESBGK model to the large Knudsen number flows is still controversial. Considering that the competition of natural convection and thermal creep mainly occurs in the slip and early transition regimes, we focus on the cases for  $0.0012 \leq Kn \leq 0.24$  in the present work. For larger Knudsen numbers, the thermal creep is dominant, and the flow pattern becomes complicated if  $Kn > 1.0$ , as demonstrated by Vargas *et al.*<sup>15</sup> This is out of the scope of the present work and can be investigated in the future.

## B. The effect of Knudsen number

Since the applicability of the USP-BGK method has been validated in both continuum and rarefied regimes, we employ it to study the gas flows in a square enclosure with temperature gradients in a wide range of the Knudsen and Froude numbers. We first study the effect of the Knudsen number on the flow patterns and heat transfer under the same Froude number condition, i.e.,  $Fr = 250.0$ . To this end, besides the two cases presented in Sec. III A, we simulate more

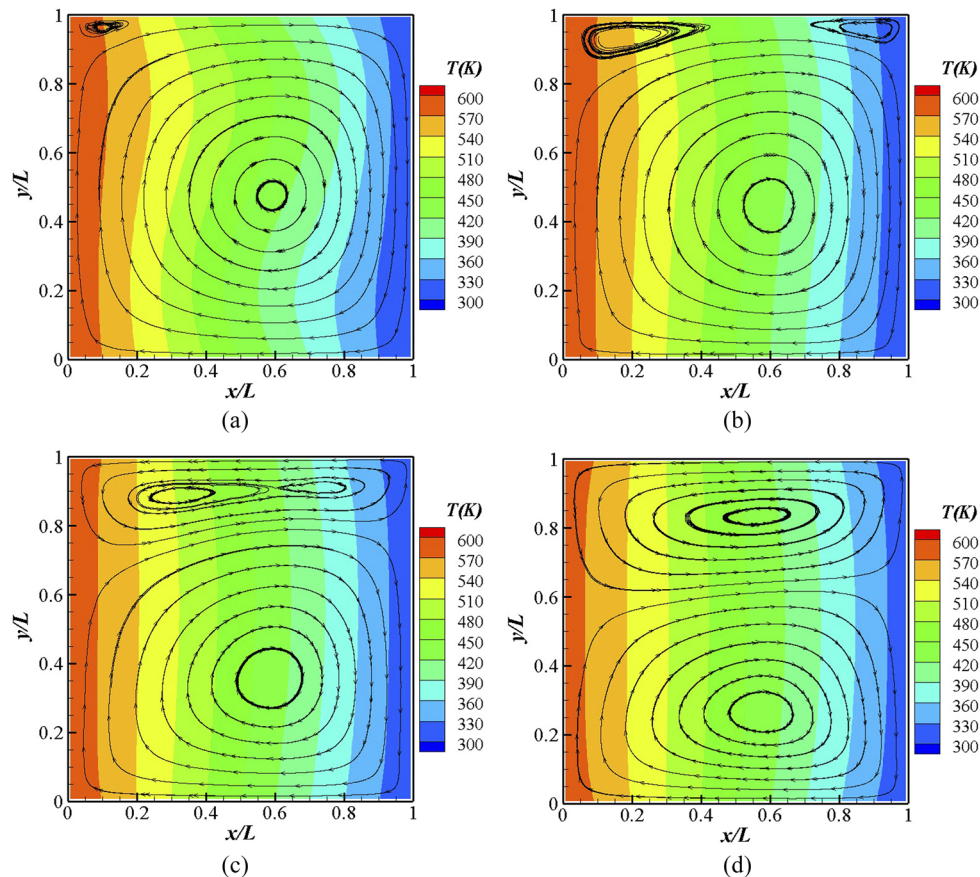


**FIG. 7.** Temperature contours and streamlines in a square enclosure at a fixed Froude number ( $Fr = 250.0$ ) and different Knudsen numbers: (a)  $Kn = 0.0023$ , (b)  $Kn = 0.0058$ , (c)  $Kn = 0.012$ , and (d)  $Kn = 0.023$ .



cases in the range of  $0.0012 < Kn < 0.12$  to cover from the continuum to the transitional regime. The required Knudsen number is reached by varying the gas density at the initial time. The temperature contours and streamlines for four typical cases are shown in Fig. 7.

For the case of  $Kn = 0.0012$ , we have seen from Fig. 2 that the one clockwise vortex is formed in the field when the effect of natural convection is dominant in the continuum regime. As the Knudsen number increases, it is interesting to note that one small vortex first emerges in the upper left corner of the enclosure, flowing along the top wall surface from the lower temperature region (right part) to the higher temperature region (left part), as shown in Fig. 7(a). This phenomenon is caused by the thermal creep mechanism due to the local rarefaction effect. Although the global Knudsen number is 0.0023 for this case, the local Knudsen numbers are about 0.0030 and 0.0013 in the top left corner and the top right corner, respectively, due to different local gas densities. Since the local Knudsen number is larger in the top left corner, the small vortex caused by thermal creep first comes out there. On the other hand, there should be the same thermal creep mechanism at the bottom wall, where the direction of the flow caused by thermal creep is the same as that caused by natural convection. Hence, the small vortex caused by thermal creep at the bottom wall is invisible due to the dominant effect of natural convection for  $Kn = 0.0023$ . More details could be found later from the velocity distributions.

When the Knudsen number increases to 0.0058, another small vortex caused by thermal creep comes out in the top right corner, as shown in Fig. 7(b). These two thermal creep vortices grow as the Knudsen number increases, and then, they merge into one big vortex in the upper half of the enclosure, as shown in Figs. 7(c) and 7(d). It should be noted that in the lower half of the enclosure, as the Knudsen number increases, the effect of thermal creep becomes more and more important. When the Knudsen number is 0.12, as shown in Fig. 4, the two big vortices in the upper and lower half of the enclosure are almost symmetric, indicating that the flow is mainly caused by thermal creep.

Figure 8 shows the distributions of the horizontal velocities in the vicinity of the top and bottom walls. For  $Kn = 0.0012$ , the horizontal velocities near the top and bottom walls are positive

and negative, respectively, following the clockwise direction of flow caused by natural convection. As the Knudsen number increases, on one hand, the flow caused by the natural convection becomes weaker. The reason for this is that the magnitude of velocity in the natural convection is proportional to the Rayleigh number, which decreases as the Knudsen number increases, as indicated in Eq. (5). On the other hand, the magnitude of the gas flows caused by thermal creep increases with the Knudsen number, and its flow direction is determined by the temperature gradient along the walls. Therefore, as the Knudsen number increases, the combined effects of weaker natural convection and stronger thermal creep need to be taken into account. Accordingly, the horizontal velocities close to the top wall gradually change from positive to negative, while the horizontal velocities close to the bottom wall are always negative, with the magnitude increasing with the Knudsen number, as shown in Fig. 8.

The effect of the Knudsen number on heat transfer is also investigated. Using molecular simulations, the heat flux at one point on a wall can be determined by taking a time average of the difference between the incident energy and reflected energy of the molecules colliding with the specific position over a time period. For the enclosure considered here, the heat flux through a wall is generated by the combination of thermal conductivity and advection. The former is proportional to the temperature gradient, while the latter depends on the flow velocity and gas density. Note that the advection in this work is caused by either natural convection or thermal creep. Figure 9 shows the normalized heat flux, i.e.,  $q/\rho(RT_{ave})^{3/2}$ , along the left wall and right wall for three different Knudsen numbers. In general, the normalized heat flux increases with the Knudsen number, and this is a common phenomenon representing the effect of Knudsen number on heat transfer.

It can be seen from Fig. 9 that the heat fluxes of the left and right walls are almost the same for the case of  $Kn = 0.12$ . They both are symmetric about the center of the height, with the minimum values at both ends, where the temperature difference between the walls and the gas is the smallest, as shown in Fig. 4. As the Knudsen number decreases, the difference of heat flux between the left and right wall gradually becomes obvious due to the asymmetric flow pattern in the horizontal direction, as shown in Fig. 7(c) for

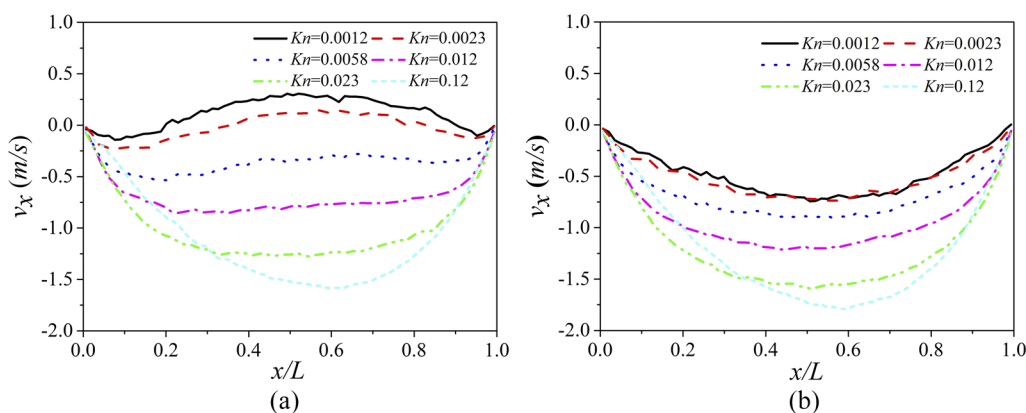


FIG. 8. Distribution of tangential velocity in the vicinity of the walls with a fixed Froude number  $Fr = 250.0$  and various Knudsen numbers: (a) top wall and (b) bottom wall.



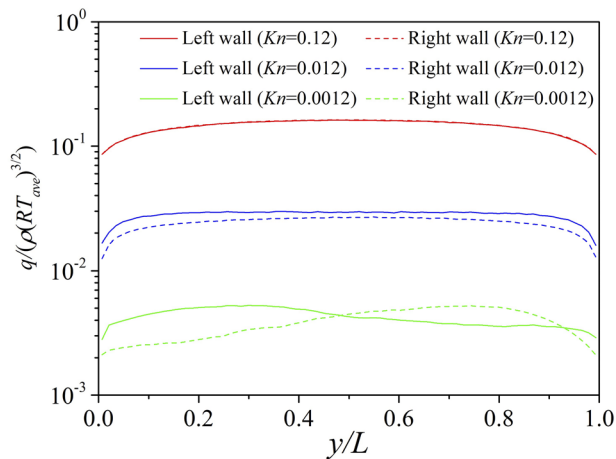


FIG. 9. Heat flux along the left wall and right wall for different Knudsen numbers.

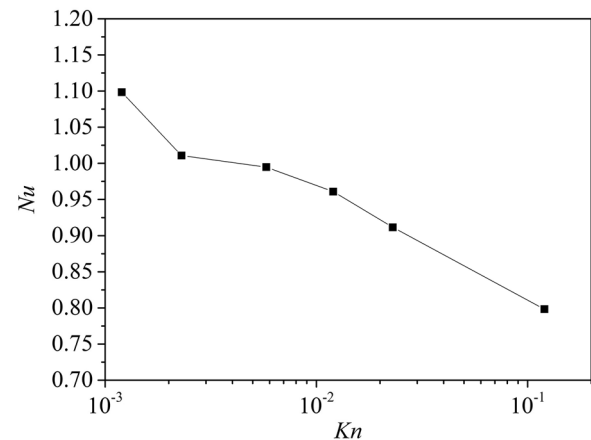


FIG. 10. Nusselt number of the left wall for different Knudsen numbers.

$Kn = 0.012$ . When the Knudsen number is 0.0012, both the heat fluxes of the left and right walls are no longer symmetric about the center of the height caused by the effect of natural convection. Specifically, the largest incident velocities normal to the left wall and the right wall are around  $y = 0.3$  and  $y = 0.8$ , respectively, as shown in Fig. 4, resulting in the maximum values of the heat fluxes at the corresponding positions.

The Nusselt number ( $Nu$ ), which is the ratio of the total heat transfer to the pure conductive heat transfer, is generally used to quantify the enhancement of heat flux due to advection. For a standard calculation of  $Nu$ , the pure conductive heat transfer should be measured under the same temperature distributions in the flow field but without any macroscopic gas motions. In molecular simulations, it is difficult to achieve only shielding the influence of velocity while keeping the other effects unchanged. Here, we simulate a simple case for each Knudsen number to be used as a reference state, where zero gravity is assumed to avoid natural convection, and symmetric boundary conditions are assumed for the top and bottom walls to avoid thermal creep. In this way, the effective Nusselt number for each case with advection is determined by the ratio of the heat flux to the corresponding value in the reference state.

Figure 10 gives the determined Nusselt number of the left wall for different Knudsen numbers. It can be seen that for the case of  $Kn = 0.0012$ , the Nusselt number is larger than 1.0, indicating that advection enhances heat transfer, and this phenomenon is well recognized in the continuum regime. As the Knudsen number increases, however, the Nusselt number goes down. The main reason for this is that the temperature distributions are greatly changed due to the existence of the top and bottom walls. Figure 11 shows the distribution of the temperature in the vicinity of the top wall along the horizontal direction for  $Kn = 0.0012$ ,  $Kn = 0.012$ , and  $Kn = 0.12$ . It can be seen that as the Knudsen number increases, the temperature close to the left wall under the condition of advection is larger than that in the reference state; in other words, the temperature difference between the left wall and the gas with advection is smaller than that in the reference state, and thus, it would result in smaller heat flux due to thermal conductivity. On the other hand, the

advection itself may also weaken the heat transfer in the rarefied regime, as reported by Rana *et al.*<sup>38</sup> These two effects result in an effective Nusselt number less than 1.0.

### C. The effect of Froude number

We next study the effect of the Froude number on the flow patterns under the same Knudsen number. Here, the geometry and the wall temperature distributions remain the same as those in Sec. II, and the gas density at the initial time instant is also invariant to keep  $Kn = 0.012$ . The change in  $Fr$  is achieved by adjusting the gravity acceleration, like the implementation in the previous studies for the Rayleigh–Bénard problem.<sup>4,34</sup>

Figure 12 shows the temperature contours and streamlines for six cases with different Froude numbers, i.e., 12.5, 25.0, 50.0, 250.0, 1250.0, and 12 500.0, corresponding to the Rayleigh numbers as 616.0, 308.0, 154.0, 30.8, 6.16, and 0.62, respectively. It can be seen that there is one clockwise vortex in the flow field for the case of

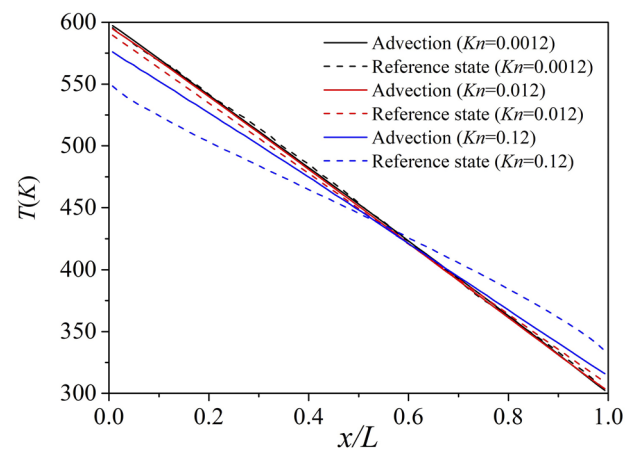
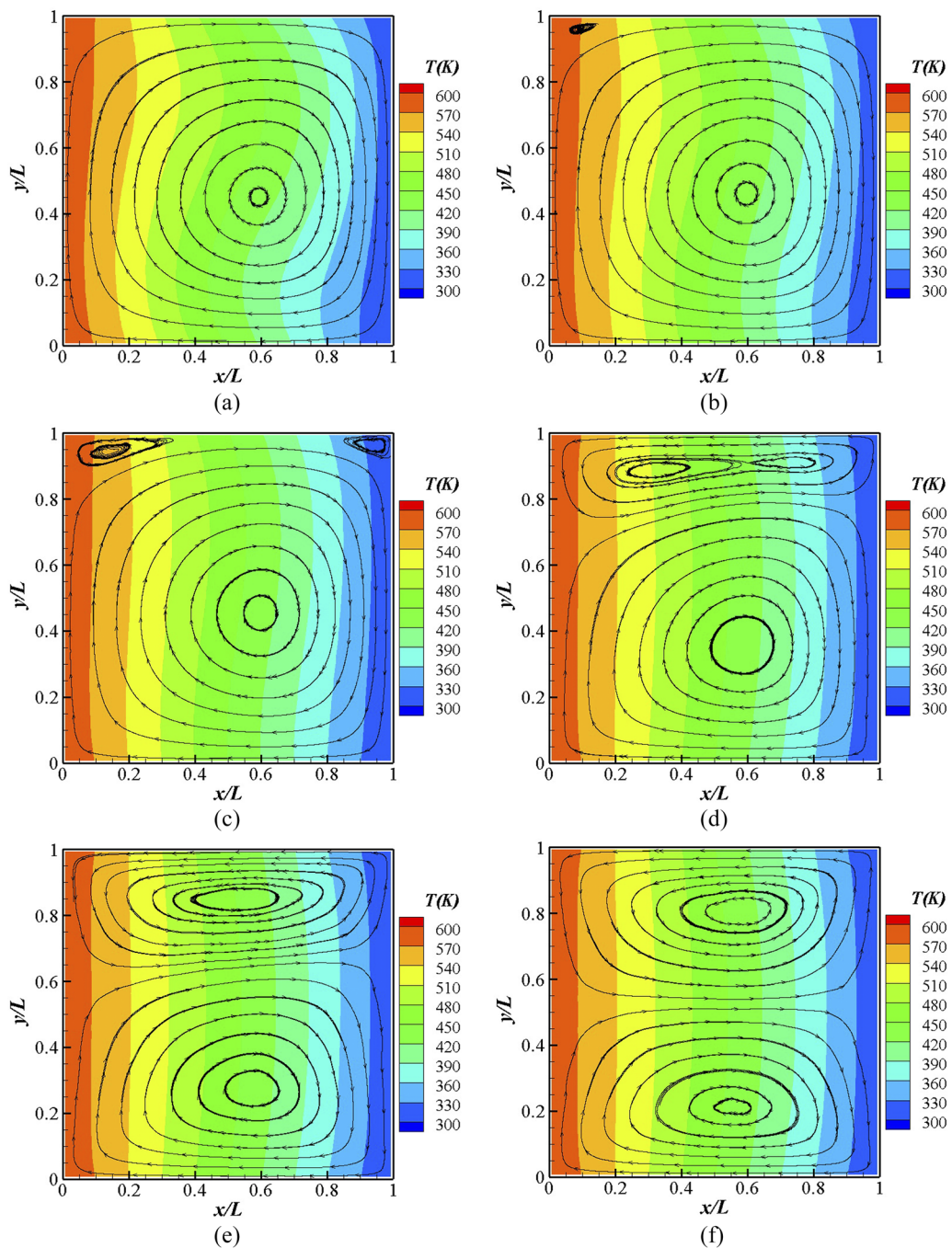


FIG. 11. Distributions of the temperature in the vicinity of the top wall along the horizontal direction for  $Kn = 0.0012$ ,  $Kn = 0.012$ , and  $Kn = 0.12$ .



**FIG. 12.** Isotherms and streamlines in a square cavity at a fixed Knudsen number ( $Kn = 0.012$ ) and various Froude numbers: (a)  $Fr = 12.5$ , (b)  $Fr = 25.0$ , (c)  $Fr = 50.0$ , (d)  $Fr = 250.0$ , (e)  $Fr = 1250.0$ , and (f)  $Fr = 12500.0$ .

$Fr = 12.5$  [Fig. 12(a)], indicating that the effect of natural convection is dominant. As the Froude number increases to 25.0, we find that one small vortex first emerges in the upper left corner of the enclosure, as shown in Fig. 12(b), caused by the thermal creep

mechanism. Then, another small vortex caused by thermal creep comes out in the top right corner for  $Fr = 50.0$ , as shown in Fig. 12(c). The sizes of these two thermal creep vortices increase with the Froude number, and they gradually merge into one big vortex in the

upper half of the enclosure, as shown in Figs. 12(d) and 12(e). When the Froude number is up to 12 500.0, it can be seen from Fig. 12(f) that the two big vortices in the upper and lower half of the enclosure are almost symmetric, indicating that the flow is mainly caused by thermal creep, and the effect of natural convection becomes negligible.

It is interesting to note that the effect of the Froude number on flow patterns is similar to the effect of the Knudsen number. On one hand, the increase in the Froude number means the decrease in the Rayleigh number, as indicated in Eq. (5), and thus, the effect of natural convection becomes weaker. On the other hand, the definition of the Froude number can be written in an alternative form as<sup>39</sup>

$$Fr = C_l^2 / gL = 2h/L, \quad (14)$$

where  $h$  is the ascent height of one free-moving molecule with the initial upward velocity of  $C_l$  in the vertical direction against gravity. In this sense, the Froude number can be thought of as a measure of the relative importance of the ascent height of molecules compared to the characteristic length of the system. Hence, the increase in the Froude number means the increase in the importance of individual molecular movements, resulting in the dominant effect of thermal creep.

#### D. Division of the (Kn, Fr) plane into domains of different flow patterns

We further carry out a parametric study of the flow patterns in a wide range of  $Kn$  and  $Fr$ , i.e.,  $0.0012 \leq Kn \leq 0.24$  and  $0.12 \leq Fr \leq 1.66 \times 10^7$ . The flow patterns are qualitatively classified into three categories: natural convection, mixed state, and thermal creep. Specifically, natural convection is defined as the state where there is one dominant vortex, and the small vortices caused by thermal creep in the upper half of the enclosure have not merged into a big one, as shown in Figs. 12(a)–12(c); thermal creep is defined as the state where there are two nearly equal vortices caused by thermal creep on the top and bottom sides, respectively, as shown in Fig. 12(f); the remaining flow patterns are defined as mixed state, as shown in Figs. 12(d) and 12(e). In Fig. 13, the flow patterns with natural convection, thermal creep, and mixed state are denoted by squares, triangles, and circles, respectively. Generally, it can be seen that small Knudsen and Froude numbers are more likely to result in natural convection, while large Knudsen and Froude numbers are more likely to result in thermal creep.

The black solid line shown in Fig. 13 is the analytic curve of  $Ra = 1.0$ , where the expression of  $Ra$  is determined by Eq. (5). It is known that the velocity caused by natural convection increases with the Rayleigh number. Consequently, if  $Ra < 1.0$ , the effect of natural convection is very weak, but the effect of thermal creep could play an important role. Figure 13 shows that when  $Kn < 0.12$ , the flow patterns on the right side of the curve of  $Ra = 1.0$  are generally thermal creep. It means that the curve of  $Ra = 1.0$  is a reasonable division between thermal creep and mixed state in the slip and continuum regimes. However, this demarcation is not applicable for  $Kn > 0.12$ , where the flow goes to the transitional regime.

On the other hand, the division of natural convection and mixed states does not seem to be determined by any isoline of the Rayleigh number. Instead, it is interesting to find that the analytic

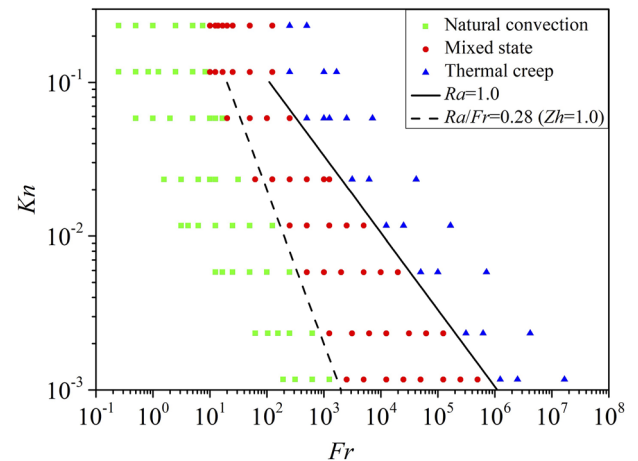


FIG. 13. Division of the (Kn, Fr) plane into domains of different flow patterns.

curve of  $Ra/Fr = 0.28$  basically separates the natural convection and mixed state when  $Kn < 0.12$ , as shown by the black dashed line in Fig. 13. Based on the computational parameters in the present work,  $Ra$  defined as Eq. (5) can be simplified as  $Ra \approx 1.1 Kn^{-2} Fr^{-1}$ , and thus,  $Ra/Fr \approx 1.1 Kn^{-2} Fr^{-2}$ . Substituting the definitions of the Knudsen number ( $Kn = \lambda/L$ ) and the Froude number [ $Fr = 2h/L$ , as shown in Eq. (14)] into the above formula, we get  $Ra/Fr \approx 1.1 L^4 / 4\lambda^2 h^2$ . In this way, the curve of  $Ra/Fr = 0.28$  can be presented in an equivalent form as  $L/\sqrt{\lambda h} \approx 1.0$ . Based on the above analysis, we propose a new nondimensional parameter to identify the flow patterns as follows:

$$Zh = L/L^* = L/\sqrt{\lambda h}, \quad (15)$$

where  $L^*$  is an equivalent characteristic length of molecules, which is the geometric mean of the molecular mean free path ( $\lambda$ ) and molecular ascent height ( $h$ ) against gravity. Natural convection is dominant when  $Zh > 1.0$ , namely, the characteristic length of the system is larger than the equivalent characteristic length of molecules. It should be noted that this criterion is also only applicable to the slip and continuum regimes but not to the transitional regime.

#### IV. CONCLUSIONS

We employed the USP-BGK method to study the competition of natural convection and thermal creep in a square enclosure for a wide range of computational parameters. Our simulation results show that the flow patterns are determined by two nondimensional parameters, i.e.,  $Kn$  and  $Fr$ , or  $Kn$  and  $Ra$ . Generally, small  $Kn$  and  $Fr$  tend to generate natural convection with one vortex in the enclosure, while large  $Kn$  and  $Fr$  tend to cause thermal creep with two vortices arrayed vertically. We further find that when  $Kn < 0.12$  (in the slip and continuum regimes), thermal creep is dominant if  $Ra < 1.0$ , while natural convection is dominant if  $Ra/Fr > 0.28$ , or equivalently,  $L/\sqrt{\lambda h} > 1.0$ . Based on this, we proposed a new nondimensional parameter, that is,  $Zh = L/\sqrt{\lambda h}$ . Our simulation results prove that  $Zh > 1.0$  is a good criterion for the importance of the effect of natural convection in the slip and continuum regimes.

In the present work, we have only studied gas flow in a square enclosure with a fixed temperature gradient. Further studies with various aspect ratios of the enclosure and temperature gradients could be done in the future. The flow patterns are expected to be more complicated in the slip and transitional regimes.

## ACKNOWLEDGMENTS

This work was supported by the National Natural Science Foundation of China (Grant No. 11772034). Results were obtained using the Tianhe-2 supercomputer.

## DATA AVAILABILITY

The data that support the findings of this study are available within the article.

## REFERENCES

- <sup>1</sup>S. Ostrach, "Natural convection in enclosures," *J. Heat Transfer* **110**, 1175 (1988).
- <sup>2</sup>S. A. Nada, "Natural convection heat transfer in horizontal and vertical closed narrow enclosures with heated rectangular finned base plate," *Int. J. Heat Mass Transfer* **50**, 667 (2007).
- <sup>3</sup>E. L. Koschmieder, *Bénard Cells and Taylor Vortices* (Cambridge University Press, 1993).
- <sup>4</sup>S. Stefanov, V. Roussinov, and C. Cercignani, "Rayleigh–Bénard flow of a rarefied gas and its attractors. I. Convection regime," *Phys. Fluids* **14**, 2255 (2002).
- <sup>5</sup>S. Stefanov, V. Roussinov, and C. Cercignani, "Rayleigh–Bénard flow of a rarefied gas and its attractors. II. Chaotic and periodic convective regimes," *Phys. Fluids* **14**, 2270 (2002).
- <sup>6</sup>A. Manela and I. Frankel, "On the Rayleigh–Bénard problem in the continuum limit," *Phys. Fluids* **17**, 036101 (2005).
- <sup>7</sup>A. Manela and I. Frankel, "On the Rayleigh–Bénard problem: Dominant compressibility effects," *J. Fluid Mech.* **565**, 461 (2006).
- <sup>8</sup>J. Zhang and J. Fan, "Monte Carlo simulation of thermal fluctuations below the onset of Rayleigh–Bénard convection," *Phys. Rev. E* **79**, 056302 (2009).
- <sup>9</sup>J. Zhang and T. Onskog, "Langevin equation elucidates the mechanism of the Rayleigh–Bénard instability by coupling molecular motions and macroscopic fluctuations," *Phys. Rev. E* **96**, 043104 (2017).
- <sup>10</sup>J. Zhang, J. Fan, and F. Fei, "Effects of convection and solid wall on the diffusion in microscale convection flows," *Phys. Fluids* **22**, 122005 (2010).
- <sup>11</sup>G. A. Bird, *Molecular Gas Dynamics and Direct Simulation of Gas Flows* (Clarendon, Oxford, 1994).
- <sup>12</sup>Y. Sone, "Flows induced by temperature fields in a rarefied gas and their ghost effect on the behavior of a gas in the continuum limit," *Annu. Rev. Fluid Mech.* **32**, 779 (2000).
- <sup>13</sup>D. H. Papadopoulos and D. E. Rosner, "Enclosure gas flows driven by non-isothermal walls," *Phys. Fluids* **7**, 2535 (1995).
- <sup>14</sup>S. Kosuge, K. Aoki, S. Takata, R. Hattori, and D. Sakai, "Steady flows of a highly rarefied gas induced by nonuniform wall temperature," *Phys. Fluids* **23**, 030603 (2011).
- <sup>15</sup>M. Vargas, G. Tatsios, D. Valougeorgis, and S. Stefanov, "Rarefied gas flow in a rectangular enclosure induced by non-isothermal walls," *Phys. Fluids* **26**, 057101 (2014).
- <sup>16</sup>J. Zhang, J. Fan, and J. Jiang, "Multiple temperature model for the information preservation method and its application to nonequilibrium gas flows," *J. Comput. Phys.* **230**, 7250 (2011).
- <sup>17</sup>P. Wang, W. Su, and L. Wu, "Thermal transpiration in molecular gas," *Phys. Fluids* **32**, 082005 (2020).
- <sup>18</sup>S. Cai, C. Cai, and J. Li, "Highly dilute gas flows through a non-isothermal planar microchannel," *Phys. Fluids* **32**, 072006 (2020).
- <sup>19</sup>Y.-L. Han and E. P. Muntz, "Experimental investigation of micro-mesoscale Knudsen compressor performance at low pressures," *J. Vac. Sci. Technol., B* **25**, 703 (2007).
- <sup>20</sup>A. A. Donkov, S. Tiwari, T. Liang, S. Hardt, A. Klar, and W. Ye, "Momentum and mass fluxes in a gas confined between periodically structured surfaces at different temperatures," *Phys. Rev. E* **84**, 016304 (2011).
- <sup>21</sup>A. Lotfian and E. Roohi, "Radiometric flow in periodically patterned channels: Fluid physics and improved configurations," *J. Fluid Mech.* **860**, 544 (2019).
- <sup>22</sup>T. Baier, S. Hardt, V. Shahabi, and E. Roohi, "Knudsen pump inspired by Crookes radiometer with a specular wall," *Phys. Rev. Fluids* **2**, 033401 (2017).
- <sup>23</sup>J. Chen, S. K. Stefanov, L. Baldas, and S. Colin, "Analysis of flow induced by temperature fields in ratchet-like microchannels by direct simulation Monte Carlo," *Int. J. Heat Mass Transfer* **99**, 672 (2016).
- <sup>24</sup>A. Patronis and D. A. Lockerby, "Multiscale simulation of non-isothermal microchannel gas flows," *J. Comput. Phys.* **270**, 532 (2014).
- <sup>25</sup>T. Zhu, W. Ye, and J. Zhang, "Negative Knudsen force on heated microbeams," *Phys. Rev. E* **84**, 056316 (2011).
- <sup>26</sup>S. Jaiswal, A. Pikus, A. Strongrich, I. B. Sebastião, J. Hu, and A. A. Alexeenko, "Quantification of thermally-driven flows in microsystems using Boltzmann equation in deterministic and stochastic contexts," *Phys. Fluids* **31**, 082002 (2019).
- <sup>27</sup>C. de Beule, G. Wurm, T. Kelling, M. Küpper, T. Jankowski, and J. Teiser, "The martian soil as a planetary gas pump," *Nat. Phys.* **10**, 17 (2014).
- <sup>28</sup>M. Schywek, J. Teiser, and G. Wurm, "Tracing thermal creep and thermophoresis in porous structures at low ambient pressure and low gravity," *Microgravity Sci. Technol.* **29**, 485 (2017).
- <sup>29</sup>T. I. Michaels and S. C. Rafkin, "Large-eddy simulation of atmospheric convection on Mars," *Q. J. R. Meteorol. Soc.* **130**, 1251 (2004).
- <sup>30</sup>A. Spiga and F. Forget, "A new model to simulate the Martian mesoscale and microscale atmospheric circulation: Validation and first results," *J. Geophys. Res.: Planets* **114**, E02009, <https://doi.org/10.1029/2008je003242> (2009).
- <sup>31</sup>H. C. Weng and C. Chen, "On the importance of thermal creep in natural convective gas microflow with wall heat fluxes," *J. Phys. D: Appl. Phys.* **41**, 115501 (2008).
- <sup>32</sup>J. Zhang, B. John, M. Pfeiffer, F. Fei, and D. Wen, "Particle-based hybrid and multiscale methods for nonequilibrium gas flows," *Adv. Aerodyn.* **1**, 12 (2019).
- <sup>33</sup>F. Fei, J. Zhang, J. Li, and Z. Liu, "A unified stochastic particle Bhatnagar–Gross–Krook method for multiscale gas flows," *J. Comput. Phys.* **400**, 108972 (2020).
- <sup>34</sup>J. Zhang and J. Fan, "Kinetic study of the Rayleigh–Bénard flows," *Chin. Sci. Bull.* **54**, 364 (2009).
- <sup>35</sup>J. Zhang, P. Tian, S. Yao, and F. Fei, "Multiscale investigation of Kolmogorov flow: From microscopic molecular motions to macroscopic coherent structures," *Phys. Fluids* **31**, 082008 (2019).
- <sup>36</sup>J. Zhang and W. Ma, "Data-driven discovery of governing equations for fluid dynamics based on molecular simulation," *J. Fluid Mech.* **892**, A5 (2020).
- <sup>37</sup>W.-L. Wang and I. D. Boyd, "Predicting continuum breakdown in hypersonic viscous flows," *Phys. Fluids* **15**, 91 (2003).
- <sup>38</sup>S. A. Rana, A. Mohammadzadeh, and H. Struchtrup, "A numerical study of the heat transfer through a rarefied gas confined in a microcavity," *Continuum Mech. Thermodyn.* **27**, 433 (2015).
- <sup>39</sup>T. Doi, "Thermal transpiration of a slightly rarefied gas through a horizontal straight pipe in the presence of weak gravitation," *Fluid Dyn. Res.* **45**, 055508 (2013).